JOURNAL OF SOLID STATE CHEMISTRY 92, 39–50 (1991)

# Structure Determinations of Two New Ternary Oxides: $Ti_3PdO$ and $Ti_4Pd_2O$

SUSAN R. LEONARD, BARRY S. SNYDER, LEO BREWER, AND ANGELICA M. STACY*

*Department of Chemistry, University of California, Berkeley, California 94720; and Materials and Chemical Sciences Division, Lawrence Berkeley Laboratory, Berkeley, California 94720*

Received July 13, 1990

Two new compounds, $Ti_3PdO$ and $Ti_4Pd_2O$, have been prepared by melting Ti, TiO, and Pd in an arc furnace, followed by annealing at 1273 K in vacuum. Both materials are deficient in palladium and have a range of oxygen stoichiometries as determined by wavelength dispersive X-ray microprobe analyses. The crystal structures were determined by profile analysis of powder X-ray diffraction data. The powder pattern of $Ti_3PdO$ was indexed based on a body-centered tetragonal unit cell with dimensions $a = 5.7247(1)$ Å, and $c = 8.3725(2)$ Å, and the structure was refined in the space group $I4/m$. This compound contains a three-dimensional network of distorted $Ti_6O$ octahedra that share corners, and is a new type of oxygen-stabilized Nowotny phase with a distorted antiperovskite structure. The powder pattern for $Ti_4Pd_2O$ was indexed based on a cubic unit cell with $a = 11.6901(1)$ Å, and the structure was refined in the space group $Fd\bar{3}m$. This compound crystallizes with the $Ti_2Ni$ structure type commonly found in other ternary oxide systems and also contains $Ti_6O$ octahedra. 

## Introduction

Many of the important heterogeneous catalysts are transition metals dispersed on oxide supports. Although the primary function of the support is to increase the surface area of the metal, there is now a vast literature documenting that supports can cause pronounced changes in the catalytic and chemisorption properties of the metal (*1–3*). In particular, when group 8–10 metals are dispersed on reducible supports such as $TiO_2$, the chemisorption properties and activity of the catalyst depend on the reduction temperature used for pretreatment. For example, the amount of hydrogen that chemisorbs at room temperature on Pd supported on $TiO_2$ decreases sharply as the reduction temperature used for pretreatment is increased from 300 to 500°C. Numerous mechanisms have been proposed to account for this suppression of chemisorption and the associated change in catalytic activity; the most popular is the diffusion of reduced $TiO_x$ moieties onto the metal, thereby blocking metal sites. However, numerous experimental observations are left unexplained by this model. For example, changes in the magnetic properties of Ni/$TiO_2$ composites with reduction temperature indicate that the Ni does not remain as elemental nickel, but forms a Ni–Ti–O

* To whom correspondence should be addressed.



0022-4596/91 $3.00

phase (*4, 5*). Unfortunately, investigations into the role of compound formation in producing the observed effect have been hindered by the fact that relatively few ternary oxides containing both an early and a late transition metal are known. The goal of our research is to find new ternary oxides that might be relevant to these catalytic systems. We report here the first two examples of reduced phases containing titanium, palladium, and oxygen.

Many metal-rich ternary metal carbides, nitrides, and oxides have structures belonging to a class known as the Nowotny octahedral phases (*6*). These $M$–$M'$–$X$ ($X$ = C, N, O) compounds are characterized by $M_6X$ octahedra which are linked either by corners, edges, or faces to form various one-, two-, or three-dimensional networks. The metal atom sublattice is not close-packed, in contrast to the binary $M$–$X$ compounds. Typically for the Nowotny phases, the $M$ element is an early transition metal, the $M'$ element is a post-transition metal, and the majority are carbides and nitrides rather than oxides. A few compounds have been discovered in which $M'$ is a late transition metal and $X$ is oxygen. In the course of our investigations into the ternary system Ti–Pd–O (*7*), we discovered two new ternary oxides which can be classified as oxygen-stabilized Nowotny phases: $Ti_3PdO$ and $Ti_4Pd_2O$.

During previous phase equilibria investigations on the ternary Ti–$M'$–O ($M'$ = Mn, Fe, Rh, Ir, Pt) (*8–10*) and Zr–$M'$–O ($M'$ = Fe, Rh, Pd, Ir, Pt) (*10*) systems, several stable ternary oxides with low oxygen content have been discovered. In each of the cases listed above, a ternary oxide forms which is isostructural with the $Ti_2Ni$ binary phase, but with the addition of oxygen in a subset of the octahedral holes formed by the Ti atoms. This structure type consists of a three-dimensional network of $M_6$ octahedra linked by sharing common faces. The nominal composition is $M_4M'_2O$, and there often exists a wide range of oxygen nonstoichiometry. In addition to the $Ti_2Ni$ structure type, there are several other structure types for ternary oxides containing an early and a late transition metal: (1) the $\kappa$-carbide type phase with nominal stoichiometry $M_9M'_4O_3$ which has been observed for the $M$–Os–O ($M$ = Zr, Hf) systems (*11*), and also as high temperature phases in the Ti–$M'$–O ($M'$ = Fe, Mn) systems (*12*); (2) the filled $D8_8$ type (or filled $Mn_5Si_3$) with nominal stoichiometry $M_5M'_3O$ which has been found in the Nb–$M'$–O ($M$ = Ir, Pt) systems (*13, 14*); (3) the filled $Re_3B$ type with nominal stoichiometry $M_3M'O$ which has been found in the Zr–Ni–O and the Hf–$M'$–O ($M'$ = Co, Ni) systems (*15*); and finally (4) the antiperovskite structure with a nominal stoichiometry of $M_3M'O$ which has been found in the Ti–Au–O and V–Au–O systems (*6*).

In this paper, we report the synthesis and crystal structures of $Ti_3PdO$ and $Ti_4Pd_2O$. The structures were determined by examination of X-ray powder diffraction data and refined by the Rietveld profile analysis method (*16*). $Ti_3PdO$ crystallizes in a new structure type that can be described best as a distorted antiperovskite. The other phase, $Ti_4Pd_2O$, was found to crystallize in the $Ti_2Ni$ structure type. It is interesting to note that superconductivity has been observed in some of the ternary oxide phases having the $Ti_2Ni$ structure type (*17*), and for $Nb_5M'_3O$ ($M'$ = Ir, Pt) (*18, 19*). The two new materials reported here do not superconduct above 2 K.

## Experimental

Samples 1 and 2 were prepared from mixtures of Ti (Noah 99.5%), TiO (Noah 99.9%), and Pd (Alfa 99.95%) powders to give Ti : Pd : O atom ratios of 32 : 9 : 9 and 59 : 29 : 12, respectively. These starting ratios were chosen to ensure that a small change in stoichiometry due to arc melting

would result in only one binary impurity phase having a simple, well-known structure, in addition to the phase of interest. Compacted powders were placed on the water-cooled hearth of an arc furnace, and melted with a nonconsumable 2% thoriated tungsten electrode under an argon atmosphere scrubbed over titanium at 300°C. Pellets of 1 and 2 were then annealed at 1273 K in a high vacuum ($10^{-6}$ Torr) furnace for 5 days and 8 days, respectively.

The compositions of the samples were determined by wavelength dispersive X-ray microprobe analysis by using high purity metal and metal oxide standards of known composition. Background, interference, and ZAF (*20*) corrections were included in the quantitative analysis. Sample 1 was found to contain predominantly a ternary phase with stoichiometry $Ti_{2.86(4)}Pd_{0.90(2)}O_{1.00(5)}$. This sample also contained a binary impurity phase having a composition within the solubility limit of oxygen in $\alpha$-Ti; the $\alpha$-Ti(O) impurity was present in sufficient quantity to be detected by X-ray diffraction. The majority of sample 2 was determined to be $Ti_{3.74(4)}Pd_{1.73(2)}O_{1.00(5)}$. This sample also was contaminated with a minor impurity phase having a composition within the solid solution range of Pd in $\beta$-Ti; this $\beta$-Ti(Pd) impurity phase was not detected by X-ray diffraction.

To check for superconductivity, magnetic measurements were performed on the powdered samples using a Quantum Design MPMS SQUID magnetometer between 2 and 20 K in an applied field of 30 Gauss.

The powder X-ray diffraction patterns used for indexing the structures were collected with a Siemens D500 diffractometer using Cu$K\alpha$ radiation. Si powder was added to the samples as an internal standard. Data were collected in the range $5° \leq 2\theta \leq 115°$ with a step size of 0.025° and count time of 10 sec. The powder X-ray diffraction profiles used for the refinement were also collected with a Siemens D500 diffractometer at ambient temperature. This diffractometer was equipped with a position-sensitive detector and a quartz crystal incident-beam monochromator to select only Cu$K\alpha_1$ radiation. Data were collected in the range $10° \leq 2\theta \leq 100°$ with a step size of 0.05° and count time of 6 sec.

## Structure Solution and Refinement

The positions of the peaks due to diffraction of the Cu$K\alpha_1$ radiation were determined for the X-ray diffraction patterns obtained for samples 1 and 2 (*21*). A zero point correction was applied, and the data were used as input for the autoindexing program TREOR (*22*). Upon exclusion of the contribution due to the $\alpha$-Ti(O) impurity phase, the remaining peaks in the powder pattern for sample 1, due to $Ti_3PdO$, were indexed satisfactorily to a tetragonal unit cell; the lattice constants refined to $a = 5.7247(1)$ Å and $c = 8.3725(2)$ Å. The only systematic absence was $h + k + l = 2n + 1$, consistent with body-centered translational symmetry. The entire diffraction pattern for sample 2, due to $Ti_4Pd_2O$, could be indexed to a cubic unit cell with a refined lattice constant of $a = 11.6901(1)$ Å. Systematic absences were consistent with the space group $Fd\bar{3}m$, suggesting the $Ti_2Ni$ structure type.

Solution of the two structures proceeded via trial and error methods for $Ti_3PdO$, and confirmation of the $Ti_2Ni$ structure type for $Ti_4Pd_2O$. The profiles were refined by the Rietveld method by using the GSAS software package (*23*). A four term Fourier series was used to describe the background; data in the range $10° \leq 2\theta \leq 18°$ were excluded from the final refinement due to a poor fit to the background. Initially, the zero point, scale factors, and cell constants were varied in the refinement. Peak shapes were refined using a pseudo-Voigtian function, including a linear Gaussian term, two nonlinear Lorentzian terms, and a small asymmetry contribution. The atomic coordinates

TABLE I

STRUCTURAL PARAMETERS AND AGREEMENT FACTORS[a]

| | $Ti_3PdO$ | $Ti_4Pd_2O$ |
|---|---|---|
| Space group | $I4/m$ | $Fd\bar{3}m$ |
| $a$(Å) | 5.7247(1) | 11.6901(1) |
| $c$(Å) | 8.3725(2) | |
| Number of background parameters | 4 | 4 |
| Number of profile parameters | 4 | 4 |
| Number of Bragg reflections | 49 | 40 |
| $R_P$[a] | 3.21 | 3.46 |
| $R_{wP}$[a] | 4.36 | 4.88 |
| $R_E$[a] | 2.60 | 2.52 |
| $R_N$[a] | 4.84 | 6.25 |

[a] $R_N = 100^*\Sigma|I_o - (1/c)I_c|/\Sigma I_o$; $R_P = 100^*\Sigma|y_{io} - (1/c)y_{ic}|/\Sigma|y_{io}|$; $R_{wP} = 100^*(\Sigma w\{y_{io} - (1/c)y_{ic}\}^2/\Sigma w\{y_{io}\}^2)^{1/2}$; $R_E = 100^*(\{N - P + C\}/w\{y_{io}\}^2)^{1/2}$, where $I$ is an integrated intensity, $y_i$ is an independent observation, $P$ is the number of least squares parameters, and $C$ is the number of constraint functions.

then were allowed to vary. For the profile refinement of sample 1, the $Ti_3PdO$ phase and the $\alpha$-Ti(O) impurity phase were refined simultaneously. The structure solution for $Ti_3PdO$ was begun in the highest symmetry of the possible space groups, $I4/mmm$. However, initial refinement of the positional parameters in $I4/mmm$ led to unsatisfactory results; refinement in $I4/m$ yielded a better fit to the pattern. For $Ti_4Pd_2O$, the origin was chosen at the $\bar{3}m$ site (origin choice 2) and the profile refinement was started using the atomic positions determined for the isostructural $Ti_4Fe_2O$ material (*8*). Isotropic thermal parameters and site occupancies were refined upon convergence of all other profile and structural parameters. For $Ti_4Pd_2O$, an attempt was made to check for filling of a second oxygen position at the 8*a* sites in the center of the undistorted $Ti_6$ octahedra. This resulted in an insignificant occupation factor and no improvement to the pattern fit.

The final values for the agreement factors and refined structural parameters are summarized in Table I. Tables II and III list the refined atom positions for $Ti_3PdO$ and $Ti_4Pd_2O$, respectively. Tables IV and V list the indexed peaks and calculated relative intensities based on the refined parameters for $Ti_3PdO$ and $Ti_4Pd_2O$, respectively. The observed, calculated, and difference profiles are shown in Figs. 1 and 2. It should be noted that the calculated values of the e.s.d.'s for the structural parameters obtained from Rietveld refinement are correlated strongly to data collection parameters (*24*), and typically are undervalued. We report these calculated e.s.d.'s throughout this paper, but recognize their limited usefulness.

## Discussion

Attempts to grow single crystals of the Ti–Pd–O ternary compounds, either by pulling crystals from the melt or by slowly cooling a melted sample in the arc furnace, resulted in polycrystalline samples containing several phases. It appears that these Ti–Pd–O ternary oxide compounds melt incongruently. The materials were synthesized, therefore, by homogenization after arc melting, which yields only powders.

TABLE II

POSITIONAL PARAMETERS FOR $Ti_3PdO$

| Atom | Site | $x$ | $y$ | $z$ | Occupancy | $U$(iso) |
|---|---|---|---|---|---|---|
| Ti(1) | 8*h* | 0.2933(53) | 0.2099(54) | 0.0000 | 1.00(1) | 0.0070(7) |
| Ti(2) | 4*e* | 0.0000 | 0.0000 | 0.2487(39) | 0.97(1) | 0.0081(0) |
| Pd | 4*d* | 0.0000 | 0.5000 | 0.2500 | 0.97(1) | 0.0079(5) |
| O(1) | 2*a* | 0.0000 | 0.0000 | 0.0000 | 1.00(3) | 0.0039(53) |
| O(2) | 2*b* | 0.0000 | 0.0000 | 0.5000 | 1.00(3) | 0.0028(52) |

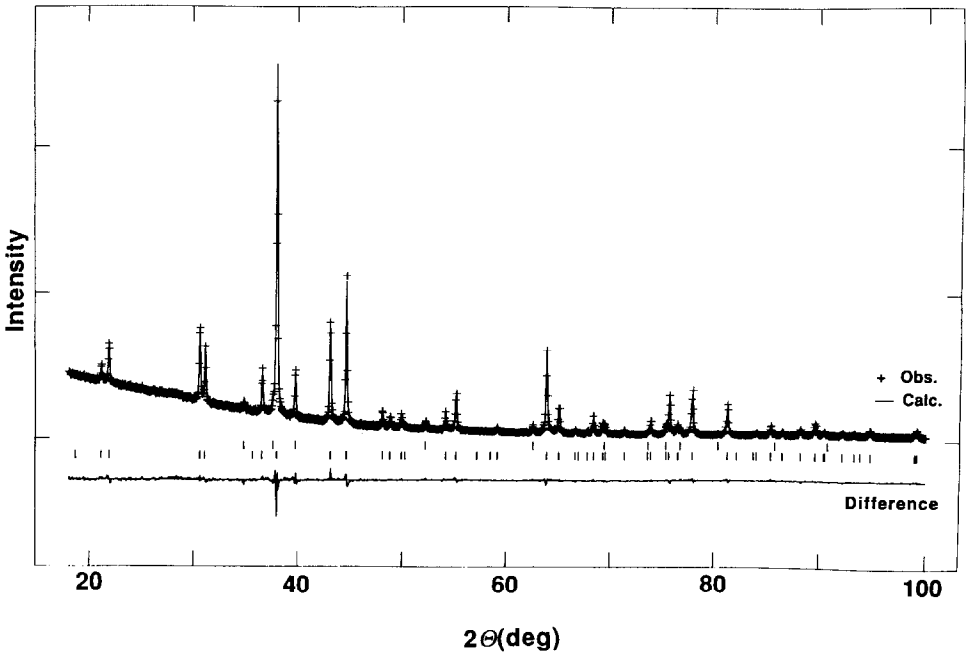


FIG. 1. X-ray diffraction pattern for $Ti_3PdO$. Observed (+) and calculated (solid line) profiles are shown along with the difference curve (lower line). Vertical markers indicate positions of Bragg reflections for $Ti_3PdO$ (lower set) and $\alpha$-Ti(O) (upper set).

*$Ti_3PdO$.* A view of the body-centered tetragonal unit cell of $Ti_3PdO$ is shown in Fig. 3. There are two crystallographically inequivalent sites for oxygen and titanium, and only one for palladium. The Pd and Ti(2) atoms form a square net in the $a$–$b$ plane at $z = \frac{1}{4}, \frac{3}{4}$. At $z = 0, \frac{1}{2}$, the O(1) and O(2) atoms also form a square net. These two types of layers are arranged with respect to each other such that the Ti(2) atoms lie above and below the O(1) and O(2) atoms; there are no atoms directly above and below the Pd atoms along the $c$ direction. The Ti(1) atoms are coplanar with and located between the O(1) and O(2) atoms, slightly closer to the O(2) atoms. Selected bond lengths and angles are given in Tables VI and VII, respectively.

A view down the $c$ axis showing the positions of the Ti and O atoms in the $Ti_3PdO$ structure is illustrated in Fig. 4. This view shows that the structure can be described in terms of a network of $Ti_6O$ octahedra. There are two different octahedra, one for each of the two types of oxygen atoms. Both O(1) and O(2) are coordinated to four Ti(1) atoms and two Ti(2) atoms. These $Ti_6O(1)$ and $Ti_6O(2)$ octahedra share corners and alternate both in the $a$–$b$ plane and along the $c$ direction, thus forming a three-dimensional network. The alternating octahedra are twisted about the $c$ axis with a dihedral angle of 18.94° between the planes defined by Ti(1)–O(1)–Ti(2) and Ti(2)–O(2)–Ti(1). This results in deviations of the Ti(1)–Ti(1)–Ti(1) bond angles from 90° between neighboring octahedra in the $a$–$b$ plane, and yields alternating values of 71.06(1)° and 108.94(1)° along the $c$ axis.

While all the Ti(1)–O–Ti(2) angles are 90°, the $Ti_6O$ octahedra are elongated slightly in the $c$ direction. The octahedra surrounding

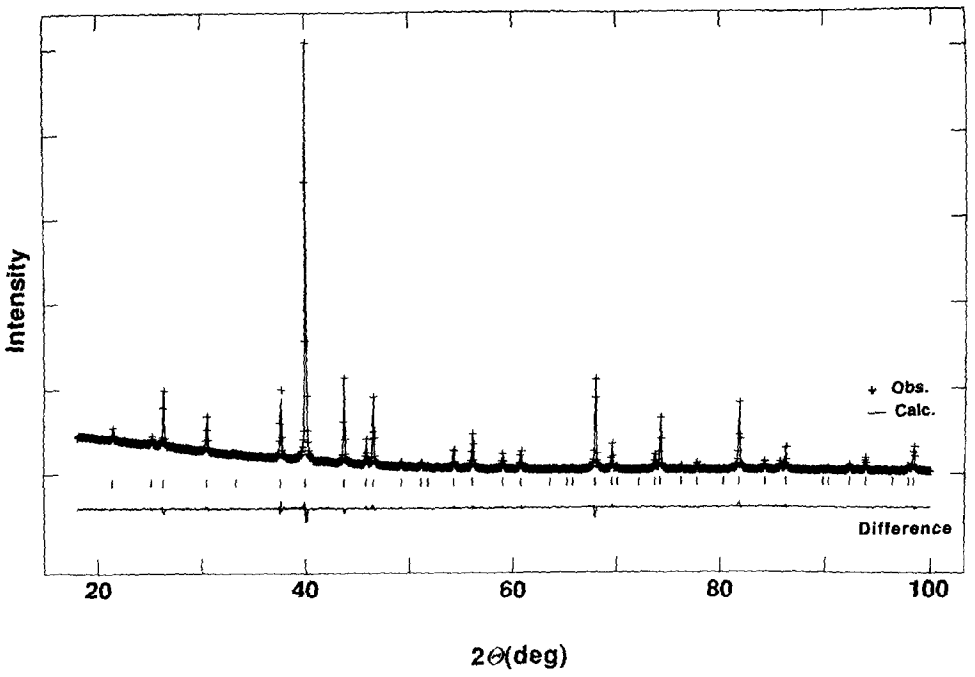


FIG. 2. X-ray diffraction pattern for $Ti_4Pd_2O$. Observed (+) and calculated (solid line) profiles are shown along with the difference curve (lower line). Vertical markers indicate positions of Bragg reflections.

the O(1) atoms are nearly regular with Ti(2)–O(1) distances of 2.082(1) Å in the *c* direction and Ti(1)–O(1) distances of 2.065(1) Å in the *a*–*b* plane. The distortion of the octahedra surrounding the O(2) atoms is only slightly greater, with Ti(2)–O(2) distances of 2.104(1) Å compared with Ti(1)–O(2) distances of 2.039(1) Å. In addition, the average Ti–O distances reported here for $Ti_3PdO$ are similar to those observed in the phases of Ti–Pd–O and Ti–Fe–O with the $Ti_2Ni$ structure type and in the $\kappa$-phase of Ti–Fe–O; in these phases the Ti–O distances range from 2.07 to 2.17 Å.

The coordination spheres about the metal atoms are rather irregular, and can best be described as distorted polyhedra. The coordination sphere around the Ti(2) atoms consists of twelve other metal atoms and two

TABLE III

POSITIONAL PARAMETERS FOR $Ti_4Pd_2O$

| Atom | Site | *x* | *y* | *z* | Occupancy | *U*(iso) |
|---|---|---|---|---|---|---|
| Ti(1) | 48*f* | 0.9446(2) | 0.1250 | 0.1250 | 1.00(1) | 0.0159(8) |
| Ti(2) | 16*d* | 0.5000 | 0.5000 | 0.5000 | 0.97(1) | 0.0048(14) |
| Pd | 32*e* | 0.2862(1) | 0.2862(1) | 0.2862(1) | 0.93(1) | 0.0036(4) |
| O | 16*c* | 0.0000 | 0.0000 | 0.0000 | 1.00(3) | 0.0211(51) |

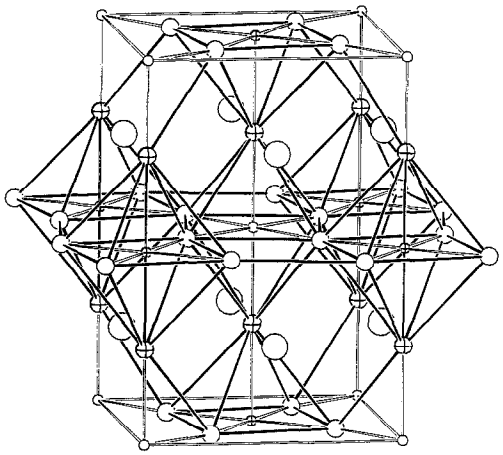

FIG. 3. A view of the unit cell of $Ti_3PdO$. The Ti(1) atoms (unshaded) and Ti(2) atoms (cross-hatched) are indicated by the intermediate size circles. The smaller circles indicate the O(1) atoms (unshaded) and the O(2) atoms (cross-hatched), and the Pd atoms are indicated by the largest circles. The Ti(1) atoms at $z = \frac{1}{2}$ extending beyond one unit cell are included to show the three-dimensional linking of the $Ti_6O$ octahedra.

oxygen atoms. The geometry of the twelve metal atoms can be characterized as a distorted cuboctahedron of eight Ti(1) and four Pd atoms. Four of the Ti(1) atoms lie above the Ti(2) atoms and four lie below; these Ti(1) atoms form parallel square faces in the $a$–$b$ plane with the faces rotated by 18.94(1)° with respect to each other. The four Pd atoms are arranged in a square around the center of the twisted prism formed by the Ti(1) atoms, thus completing the distorted cuboctahedron. The Ti(2)–Pd distance and all Ti–Ti distances are approximately 2.9 Å; this is comparable to distances observed in the binary intermetallics (*25*). In addition to the coordination of twelve metal atoms, each Ti(2) atom is also bonded to one O(1) and one O(2) atom located in the centers of the square faces formed by the Ti(1) atoms. Because the Ti(1)–O(1) distances are slightly larger than the Ti(1)–O(2) distances, the squares formed by the Ti(1) atoms are not equal in size.

The coordination geometry around the Pd atoms is somewhat similar to that described for the Ti(2) atoms. There are twelve metal atoms in the coordination sphere, eight Ti(1) and four Ti(2) atoms, but no oxygen atoms are bonded to the Pd atoms. The symmetry is lower compared with the metal atom geometry around Ti(2) because the parallel faces of the prism formed by the eight Ti(1) atoms are not square. The significant distortion to the cuboctahedral environment is also evident from the wide range of Ti–Pd

TABLE IV

POWDER DIFFRACTION PATTERN FOR $Ti_3PdO$

| $h\ k\ l$ | $I/I_{max}$ | $d$(Å) |
|---|---|---|
| 0 0 2 | 4 | 4.186 |
| 1 1 0 | 11 | 4.048 |
| 1 1 2 | 20 | 2.910 |
| 2 0 0 | 15 | 2.862 |
| 2 1 1 | 10 | 2.448 |
| 2 0 2 | 100 | 2.363 |
| 0 0 4 | 25 | 2.093 |
| 2 2 0 | 37 | 2.024 |
| 2 1 3 | 4 | 1.887 |
| 1 1 4 | 3 | 1.859 |
| 2 2 2 | 5 | 1.822 |
| 3 1 0 | 1 | 1.810 |
| 2 0 4 | 6 | 1.690 |
| 3 1 2 | 11 | 1.662 |
| 3 2 1 | 1 | 1.560 |
| 2 2 4 | 23 | 1.455 |
| 4 0 0 | 9 | 1.431 |
| 2 1 5 | 2 | 1.401 |
| 3 2 3 | 1 | 1.380 |
| 4 1 1 | 4 | 1.370 |
| 3 1 4 | 1 | 1.369 |
| 4 0 2 | 3 | 1.354 |
| 3 3 0 | 1 | 1.350 |
| 1 1 6 | 1 | 1.319 |
| 4 2 0 | 4 | 1.280 |
| 2 0 6 | 12 | 1.254 |
| 4 1 3 | 3 | 1.243 |
| 4 2 2 | 15 | 1.224 |
| 4 0 4 | 9 | 1.181 |
| 2 2 6 | 1 | 1.149 |
| 4 3 1 | 1 | 1.134 |
| 3 3 4 | 2 | 1.134 |
| 5 1 0 | 1 | 1.123 |
| 3 1 6 | 3 | 1.105 |
| 4 2 4 | 5 | 1.092 |
| 5 1 2 | 1 | 1.084 |
| 2 1 7 | 1 | 1.084 |
| 4 1 5 | 2 | 1.069 |
| 4 3 3 | 1 | 1.059 |
| 0 0 8 | 2 | 1.047 |
| 1 1 8 | 1 | 1.013 |
| 4 4 0 | 2 | 1.012 |

TABLE V

POWDER DIFFRACTION PATTERN FOR $Ti_2Pd_4O$

| *h k l* | $I/I_{max}$ | *d*(Å) |
|---|---|---|
| 1 1 1 | 29 | 6.749 |
| 2 2 0 | 6 | 4.133 |
| 3 1 1 | 4 | 3.525 |
| 2 2 2 | 27 | 3.375 |
| 4 0 0 | 17 | 2.923 |
| 3 3 1 | 1 | 2.682 |
| 4 2 2 | 29 | 2.387 |
| 5 1 1 | 100 | 2.250 |
| 3 3 3 | 49 | 2.250 |
| 4 4 0 | 31 | 2.067 |
| 5 3 1 | 9 | 1.976 |
| 4 4 2 | 26 | 1.948 |
| 6 2 0 | 2 | 1.848 |
| 5 3 3 | 2 | 1.783 |
| 6 2 2 | 1 | 1.762 |
| 4 4 4 | 6 | 1.687 |
| 7 1 1 | 14 | 1.637 |
| 5 5 1 | 3 | 1.637 |
| 6 4 2 | 6 | 1.562 |
| 7 3 1 | 7 | 1.522 |
| 5 5 3 | 1 | 1.522 |
| 6 6 0 | 29 | 1.378 |
| 8 2 2 | 6 | 1.378 |
| 5 5 5 | 9 | 1.350 |
| 6 6 2 | 1 | 1.341 |
| 9 1 1 | 3 | 1.283 |
| 7 5 3 | 2 | 1.283 |
| 8 4 2 | 18 | 1.276 |
| 6 6 4 | 1 | 1.246 |
| 9 3 1 | 3 | 1.226 |
| 9 3 3 | 19 | 1.175 |
| 7 5 5 | 6 | 1.175 |
| 10 2 0 | 3 | 1.146 |
| 9 5 1 | 1 | 1.130 |
| 7 7 3 | 2 | 1.130 |
| 10 2 2 | 8 | 1.125 |
| 8 6 4 | 1 | 1.085 |
| 10 4 2 | 2 | 1.067 |
| 7 7 5 | 5 | 1.054 |
| 9 7 1 | 1 | 1.021 |
| 9 5 5 | 1 | 1.021 |
| 8 8 2 | 8 | 1.018 |
| 10 4 4 | 2 | 1.018 |

distances of 2.688(1) Å to 3.156(1) Å. The average Ti–Pd distance, 2.90 Å, is similar to that found in the $Ti_4Pd_2O$ phase described below and in the binary Ti–Pd intermetallics (*25*).

The geometry of the twelve metal atoms around the Ti(1) atoms, consisting of four Ti(2), four Pd, and four Ti(1) atoms can be considered at best an extremely distorted cuboctahedron. Two Ti(2) and two Pd atoms form a square above and below each Ti(1) atom. Four Ti(1) atoms are arranged in a trapezoid around the center of this prism. The Ti(1) atom is displaced from the center of the metal coordination sphere by 0.059(1) Å in the *a–b* plane. In addition to the twelve metal atoms, the coordination sphere of the Ti(1) atoms also contains one O(1) and one O(2) atom.

TABLE VI

SELECTED BOND LENGTHS (Å) FOR $Ti_3PdO$

| Atom 1 | Atom 2 | Distance |
|---|---|---|
| O(1) | Ti(1) × 4 | 2.065(1) |
| O(1) | Ti(2) × 2 | 2.082(1) |
| O(2) | Ti(1) × 4 | 2.039(1) |
| O(2) | Ti(2) × 2 | 2.104(1) |
| Pd | Ti(1) × 4 | 3.156(1) |
| Pd | Ti(1) × 4 | 2.688(1) |
| Pd | Ti(2) × 4 | 2.862(1) |
| Ti(1) | Ti(1) × 2 | 2.920(1) |
| Ti(1) | Ti(1) × 2 | 2.884(1) |
| Ti(1) | Ti(2) × 2 | 2.930(1) |
| Ti(1) | Ti(2) × 2 | 2.932(1) |
| Ti(1) | Pd × 2 | 3.156(1) |
| Ti(1) | Pd × 2 | 2.688(1) |
| Ti(1) | O(1) × 1 | 2.065(1) |
| Ti(1) | O(2) × 1 | 2.039(1) |
| Ti(2) | Ti(1) × 4 | 2.930(1) |
| Ti(2) | Ti(1) × 4 | 2.932(1) |
| Ti(2) | Pd × 4 | 2.862(1) |
| Ti(2) | O(1) × 1 | 2.082(1) |
| Ti(2) | O(2) × 1 | 2.104(1) |

Holding the occupancy of the Ti(1) atoms fixed at 1.00, the refined stoichiometry was determined to be $Ti_{2.97}Pd_{0.97}O_{1.00}$, in reason-

TABLE VII

SELECTED BOND ANGLES (°) FOR $Ti_3PdO$

| Atom 1 | Atom 2 | Atom 3 | Angle |
|---|---|---|---|
| Ti(1) | O(1) | Ti(1) | 90.00 |
| Ti(1) | O(1) | Ti(2) | 90.00 |
| Ti(1) | O(2) | Ti(1) | 90.00 |
| Ti(1) | O(2) | Ti(2) | 90.00 |
| Ti(1) | Ti(1) | Ti(1) | 90.00 × 2 |
| Ti(1) | Ti(1) | Ti(1) | 71.06(1) |
| Ti(1) | Ti(1) | Ti(1) | 108.94(1) |

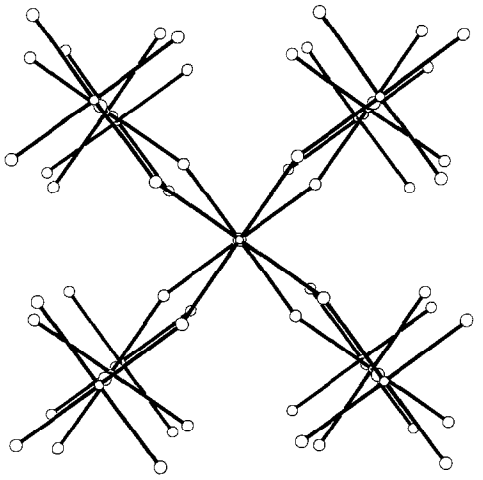

FIG. 4. A portion of the Ti (large circles) and O (small circles) sublattice of $Ti_3PdO$ projected down the $c$ axis of the unit cell, showing the three-dimensional network of corner-shared $Ti_6O$ octahedra.

able agreement with the microprobe results. This stoichiometry corresponds to a Ti/Pd atom ratio of approximately 3.06, compared with 3.18 from the microprobe data. Attempts to determine phase boundaries have shown that there is a fixed Ti/Pd atom ratio for which the structure is stable. If the Ti/Pd atom ratio is smaller than ~3.1, then $Ti_4Pd_2O$ coexists with $Ti_3PdO$ in equilibrium at 1273 K. For larger Ti/Pd atom ratios, $Ti_3PdO$ is in equilibrium with the $\alpha$-Ti(O) phase. The $Ti_3PdO$ phase in the sample used for the refinement had a composition with the maximum oxygen stoichiometry for which the $Ti_3PdO$ phase is stable; the range of oxygen nonstoichiometry is approximately 5 at% O as determined by microprobe.

As is apparent from the description of the $Ti_3PdO$ structure, this is a new type of oxygen-stabilized Nowotny phase. The phases most closely related are the $M_3M'X$ compounds with the cubic antiperovskite structure (*6*). In the antiperovskite structure the $M_6X$ octahedral units are linked by sharing corners with six neighboring octahedra to form a three-dimensional network of fourfold channels. Similar linking of the octahedral units in the $Ti_3PdO$ structure leads to this same basic network. Due to the fact that the Ti atoms are on positions of lower symmetry, the channels do not have fourfold symmetry. In both structure types, the $M'$ atoms are located in the void formed by eight of the connected $M_6X$ units. Therefore, the $Ti_3PdO$ structure type can be viewed as a distorted antiperovskite structure.

Various distortions from the cubic symmetry of the antiperovskite structure have been observed, including those found in $Cr_3GeN$ (*26*) and $Cr_3AsN$ (*27*). The former crystallizes in the space group $P\bar{4}2_1m$ with lattice parameters $a$ = 5.375 Å and $c$ = 4.012 Å. The Cr(1) and $M'$ atoms are displaced slightly from the positions they would occupy in an ideal antiperovskite structure. Also, the octahedra are rotated with respect to each other in the $a$–$b$ plane, but are coincident in the $c$ direction. $Cr_3AsN$ crystallizes in the space group $I4/mcm$ in the filled $U_3Si$ structure type with lattice parameters $a$ = 5.360 Å and $c$ = 8.066 Å. Although there is a single type of $M_6X$ octahedron, this structure deviates from the antiperovskite structure due to a rotation of the $Cr_6N$ octahedra relative to each other in both the $a$–$b$ plane and the $c$ direction. Two other ternary nitride phases, $M_3GeN$ ($M$ = Mn, Fe), and a carbide phase, $Mn_3GeC$, have also been reported (*27*) to be isostructural with $Cr_3AsN$. The structure of $Ti_3PdO$ is very similar to the filled $U_3Si$ structure type, but deviates even further from the ideal antiperovskite structure. As described above, there are two inequivalent octahedral units in $Ti_3PdO$, and thus two different oxygen environments. Finally, the range of metal–metal distances is larger than in the $U_3Si$ structure type.

*$Ti_4Pd_2O$.* This crystallizes in the $Ti_2Ni$ structure type, detailed descriptions of which can be found elsewhere (*6, 11*). In the

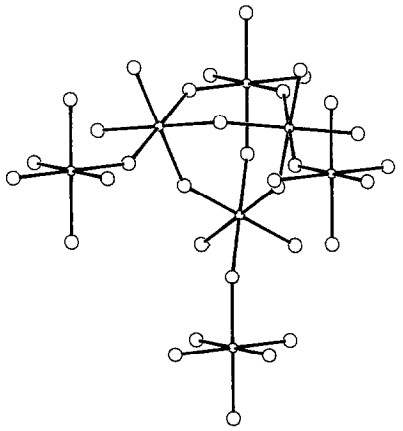

FIG. 5. A portion of the Ti(1) (large circles) and O (small circles) sublattice of $Ti_4Pd_2O$ showing the three-dimensional network of corner shared $Ti(1)_6O$ octahedra.

large face-centered cubic unit cell of 11.6901(1) Å, there are two unique titanium sites, a single palladium site, and one type of oxygen site. The structure can be described as two interpenetrating sublattices, one consisting of the Ti(1) and O atoms, the other containing the Ti(2) and Pd atoms. Views of these sublattices are shown in Figs. 5 and 6, respectively. Selected bond lengths and angles are given in Tables VIII and IX, respectively.

The Ti(1) sublattice in $Ti_4Pd_2O$ can be described as a three-dimensional network of face sharing $Ti(1)_6$ octahedra. There are two different $Ti(1)_6$ octahedral sites which could be occupied by the oxygen atoms. One is centered around the 8*a* positions and is regular. The other octahedron, centered around the 16*c* position, deviates from regularity by having unequal Ti(1)–Ti(1) bond lengths. These two different $Ti(1)_6$ units alternate throughout the structure, and only the 16*c* site is occupied. The view of the Ti(1) and O atoms in Fig. 5 shows that consideration of only the filled octahedra leads to the alternate description of $Ti_4Pd_2O$ as a three-dimensional network of corner-sharing $Ti(1)_6O$ units. While the $Ti_6O$ octahedra have equal Ti(1)–O bond lengths, two of the Ti(1)–O–Ti(1) angles are 87.03(1)° and two are 92.97(1).° These angular distortions are only slightly greater than those found in the isostructural $Ti_4Fe_2O$ material of 89.43° and 90.57° (*8*). The Ti(1)–O bond distance of

TABLE VIII

SELECTED BOND LENGTHS (Å) FOR $Ti_4Pd_2O$

| Atom 1 | Atom 2 | Distance |
|---|---|---|
| O | Ti(1) × 6 | 2.166(1) |
| Pd | Ti(1) × 3 | 3.072(1) |
| Pd | Ti(1) × 3 | 2.675(1) |
| Pd | Ti(2) × 3 | 2.570(1) |
| Pd | Pd × 3 | 2.935(1) |
| Ti(1) | Ti(1) × 4 | 3.141(1) |
| Ti(1) | Ti(1) × 4 | 2.982(1) |
| Ti(1) | Ti(2) × 2 | 3.074(1) |
| Ti(1) | Pd × 2 | 2.675(1) |
| Ti(1) | Pd × 2 | 3.072(1) |
| Ti(1) | O × 2 | 2.166(1) |
| Ti(2) | Ti(1) × 6 | 3.074(1) |
| Ti(2) | Pd × 6 | 2.570(1) |

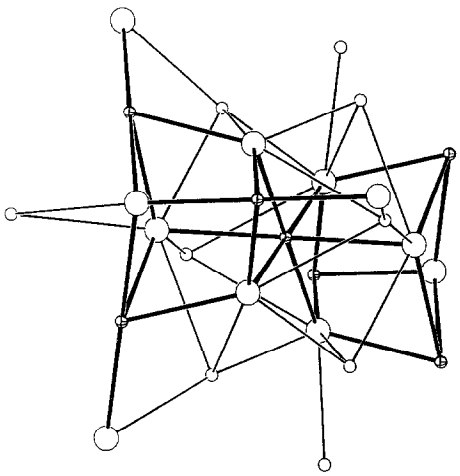

FIG. 6. A portion of the Ti(2) (cross-hatched) and Pd (large unshaded circles) sublattice of $Ti_4Pd_2O$ showing the two interpenetrating homometallic tetrahedra (connected by bold lines). Some of the Ti(1) atoms (small unshaded circles) are included.

TABLE IX

SELECTED BOND ANGLES (°) FOR $Ti_4Pd_2O$

| Atom 1 | Atom 2 | Atom 3 | Angle |
|---|---|---|---|
| Ti(1) | O | Ti(1) | 87.03(1) × 2 |
| Ti(1) | O | Ti(1) | 92.97(1) × 2 |
| Ti(1) | O | Ti(1) | 180.00 |

2.166(1) Å is similar to that found in $Ti_4Fe_2O$ (2.130 Å).

The Pd/Ti(2) sublattice consists of Pd and Ti(2) atoms arranged in interpenetrating homometallic tetrahedra. Because these two tetrahedra are of differing sizes, the $Ti(2)_4Pd_4$ unit shown in Fig. 6 is best described as a cubanoid. These cubanoids are linked in a three-dimensional network by corner sharing of the Ti(2) atoms.

As was the case for $Ti_3PdO$, the coordination spheres about the metal atoms in $Ti_4Pd_2O$ are irregular. The Ti(2) atoms are located in an approximately icosahedral environment consisting of six Ti(1) and six Pd atoms. Each Pd atom is coordinated by the three other Pd atoms making up the tetrahedron and also by six Ti(1) and three Ti(2) atoms. The Ti–Pd bond lengths range from 2.570(1) Å to 3.072(1) Å, averaging 2.77 Å, which is comparable to the usual 2.7 to 2.9 Å Ti–Pd distances found in the binary intermetallics (*25*). The Ti–Ti distances and Pd–Pd distances are also similar to those observed in the binary intermetallics (*25*). The geometry about the Ti(1) atoms is highly irregular.

Holding the occupancy for Ti(1) at 1.00, the refined stoichiometry is $Ti_{3.97}Pd_{1.86}O_{1.00}$. The refined Ti/Pd atom ratio of 2.13 is in excellent agreement with the ratio 2.16 found by microprobe analysis. This stoichiometry corresponds to totally filled oxygen 16*c* sites, and empty 8*a* sites. Phase boundary determinations by microprobe analysis of samples containing this phase and those in equilibrium with it (*7*) indicate that $Ti_4Pd_2O$ only exists for a fixed Ti/Pd atom ratio. This is in contrast to other isostructural materials; for example, in the Ti–Fe–O system (*28*), the $Ti_2Ni$-type structure exists for a Ti/Fe atom ratio of 2 to a stoichiometry $Ti_3Fe_3O$. For Ti/Fe ratios less than 2, the Fe substitutes at the Ti 16*d* sites. The stoichiometry $Ti_{3.78(4)}Pd_{1.70(2)}O_{1.42(5)}$ was determined by microprobe analysis to be the upper oxygen limit for which the phase is stable. This stoichiometry could be accommodated by either adding additional vacancies on the metal sites or filling the regular octahedra (8*a* sites) with oxygen.

## Conclusions

Prior to this investigation, only three ternary oxides containing titanium and a late transition metal had been reported: $Ti_4Rh_2O$, $Ti_4Ir_2O$, and $Ti_4Pt_2O$. All of these phases have the $Ti_2Ni$ structure type. We have shown that $Ti_4Pd_2O$ also forms with the same structure type, but the material is slightly deficient in Pd. In addition, we have discovered a second reduced oxide in the Ti–Pd–O system, $Ti_3PdO$, with a distorted antiperovskite structure. We have found that these reduced ternary oxides have a very large thermochemical stability (*7*); this is not surprising because of the extreme thermochemical stability of the binary metal intermetallics consisting of an early and a late transition metal (*29*), and the strong affinity of the early transition metals for oxygen. Because of this large stability, these reduced oxides might form when Rh, Ir, Pd, and Pt metals are supported on $TiO_2$ and subsequently treated in hydrogen at elevated temperatures. Certainly, the catalytic activity of these reduced ternary oxides should be examined.

## Acknowledgments

This work was supported by the Director, Office of Basic Energy Research, Office of Basic Energy Sciences, Materials Science Division of the United States

Department of Energy under Contract DE-AC03-76SF0009. The authors thank S. Justi, K. Schwartz, and M. Thompson at Raychem for collecting the X-ray diffraction data. A.M.S. thanks the Alfred P. Sloan Foundation and the Camille and Henry Dreyfus Foundation for their support.

## References

1. G. L. HALLER AND D. E. RESASCO, *in* "Advances in Catalysis," (D. D. Eley, H. Pines, and P. B. Weisz, Eds.), p. 173, Academic Press, New York (1989).
2. S. J. TAUSTER, *Acc. Chem. Res.* **20,** 389 (1987).
3. R. T. K. BAKER, S. J. TAUSTER, AND J. A. DUMESIC (Eds.), "Strong Metal Support Interactions," ACS Symposium Series 298; American Chemical Society, Washington D.C. (1986).
4. H.-C. ZUR LOYE AND A. M. STACY, *Langmuir* **4,** 1261 (1988).
5. H.-C. ZUR LOYE AND A. M. STACY, *J. Amer. Chem. Soc.* **107,** 4567 (1985).
6. L. E. TOTH, "Transition Metal Carbides and Nitrides," Academic Press, New York (1971).
7. S. R. LEONARD AND L. BREWER, in press.
8. B. RUPP AND P. FISCHER, *J. Less-Common Metals* **144,** 275 (1988).
9. M. V. NEVITT, *Trans. Metall. Soc. AIME* **218,** 327 (1960).
10. M. V. NEVITT, J. W. DOWNEY, AND R. A. MORRIS, *Trans. Metall. Soc. AIME* **218,** 1019 (1960).
11. P. ROGL AND H. NOWOTNY, *Monatsh. Chem.* **108,** 1167 (1976).
12. P. ROGL, B. RUPP, G. WIESINGER, J. SCHEFER, AND P. FISCHER, *J. Less-Common Metals* **113,** 103 (1985).
13. R. HORYN AND L. FOLCIK-KOKOT, *J. Less-Common Metals* **57,** 75 (1978).
14. R. HORYN AND R. ANDRUSZKIEWICZ, *J. Less-Common Metals* **71,** 9 (1980).
15. H. BOLLER, *Monatsh. Chem.* **104,** 545 (1973).
16. H. M. RIETVELD, *J. Appl. Crystallogr.* **2,** 65 (1969).
17. B. T. MATTHIAS, T. H. GEBALLE, AND V. B. COMPTON, *Rev. Mod. Physics* **35,** 1 (1963).
18. R. HORYN, L. FOLCIK-KOKOT, AND N. ILIEV, *J. Less-Common Metals* **57,** 69 (1978).
19. B. CORT, A. L. GIORGI, AND G. R. STEWART, *J. Low Temp. Physics* **47,** 179 (1981).
20. V. D. SCOTT AND G. LOVE (Eds.), "Quantitative Electron-Probe Analysis," Ellis Horword Limited: West Sussex, England (1983).
21. Siemens "DIFFRAC-AT Software Package." SOCABIM (1986).
22. P. E. WERNER, *Z. Krystallogr.* **120,** 375 (1964).
23. A. C. LARSON AND R. B. VON DREELE, "GSAS-Generalized Crystal Struct. Anal. Syst." Los Alamos Report LAUR 86-748, Los Alamos Natl. Lab.
24. R. J. HILL AND I. C. MADSEN, *J. Appl. Crystallogr.* **19,** 10 (1986).
25. J. L. MURRAY, "Bulletin of Alloy Phase Diagrams," Vol. 3, No. 3, p. 321 (1982).
26. H. BOLLER, *Monatsh. Chem.* **100,** 1477 (1969).
27. H. BOLLER, *Monatsh. Chem.* **99,** 2444 (1968).
28. B. RUPP, *J. Less-Common Metals* **104,** 51 (1984).
29. L. TOPOR AND O. J. KLEPPA, *J. Chem. Thermodyn.* **20,** 1271 (1988), and references therein.